2011-05

Wind Stress Curl and Coastal Upwelling in the Area of Monterey Bay Observed during AOSN-II

Wang, Q.

Wind Stress Curl and Coastal Upwelling in the Area of Monterey Bay Observed during AOSN-II

Q. WANG

Naval Postgraduate School, Monterey, California

J. A. KALOGIROS

National Observatory of Athens, Athens, Greece

S. R. RAMP

Monterey Bay Aquarium Research Institute, Moss Landing, California

J. D. PADUAN, G. BUZORIUS, AND H. JONSSON

Naval Postgraduate School, Monterey, California

ABSTRACT

Aircraft measurements obtained during the 2003–04 Autonomous Ocean Sampling Network (AOSN-II) project were used to study the effect of small-scale variations of near-surface wind stress on coastal upwelling in the area of Monterey Bay. Using 5-km-long measurement segments at 35 m above the sea surface, wind stress and its curl were calculated with estimated accuracy of 0.02–0.03 N m^{-2} and 0.1–0.2 N m^{-2} per 100 kilometers, respectively. The spatial distribution of wind speed, wind stress, stress curl, and sea surface temperature were analyzed for four general wind conditions: northerly or southerly wind along the coastline, onshore flow, and offshore flow. Wind stress and speed maxima frequently were found to be noncollocated as bulk parameterizations imply owing to significant stability and nonhomogeneity effects at cold SST pools. The analyses revealed that complicated processes with different time scales (wind stress field variation, ocean response and upwelling, sea surface currents, and heating by solar radiation) affect the coastal sea surface temperature. It was found that the stress-curl-induced coastal upwelling only dominates in events during which positive curl extended systematically over a significant area (scales larger than 20 km). These events included cases with a northerly wind, which resulted in an expansion fan downstream from Point Año Nuevo (wind speed peaks greater than about 8–10 m s^{-1}), and cases with an offshore/onshore flow, which are characterized by weak background upwelling due to Ekman transport. However, in general, observations show that cold pools of sea surface temperature in the central area of Monterey Bay were advected by ocean surface currents from strong upwelling regions. Aircraft vertical soundings taken in the bay area showed that dominant effects of the lee wave sheltering of coastal mountains resulted in weak atmospheric turbulence and affected the development of the atmospheric boundary layer. This effect causes low wind stress that limits upwelling, especially at the northern part of Monterey Bay. The sea surface temperature is generally warm in this part of the bay because of the shallow oceanic surface layer and solar heating of the upper ocean.

Corresponding author address: Dr. John Kalogiros, Institute of Environmental Research and Sustainable Development, National Observatory of Athens, Lofos Koufou, P. Penteli, Athens 15236, Greece.
E-mail: jkalog@meteo.noa.gr

1. Introduction

Wind stress is an important forcing of sea surface perturbations, either as waves or as surface currents, and it drives coastal upwelling through the divergence of surface Ekman transport. Upwelling may occur near the

coast due to the presence of a coastal boundary, a process that will be referred to as "Ekman transport." Ekman pumping is due to the curl of wind stress or, equivalently, the divergence of the Ekman transport (Kraus and Businger 1994) and may cause upwelling nearshore or offshore. Along the west coast of major continents in the Northern Hemisphere, such as the coastal California region, northerly winds along the coast favor coastal upwelling through Ekman transport. The upwelling effects of Ekman transport may extend to large scales alongshore $O(100 \text{ km})$ and in the coastal zone (~20 km offshore). Its indirect effects can be seen typically in satellite SST images as filaments of cold water rich in chlorophyll, which are formed because of possible baroclinic instability of the front of the cold upwelling water and extend more than 100 km offshore. Positive wind stress curl is expected to enhance upwelling locally on scales $O(10 \text{ km})$ through Ekman pumping. The focus of this work is on the latter: upwelling through positive wind stress curl in the coastal zone. The upwelling rate due to Ekman transport may be as high as 9 m day^{-1} in strong upwelling centers (Pickett and Paduan 2003; Enriquez and Friehe 1995) while, on average, along the California coast it may be only 1–2 m day^{-1}. The upwelling rate due to Ekman pumping, which far offshore is directly proportional to wind stress curl (Kraus and Businger 1994), can increase to 17 m day^{-1} in strong upwelling centers.

The large-scale wind stress field over the ocean is usually estimated indirectly from buoy or shipboard measurements (Winant and Dorman 1997) or atmospheric models (Tjernström and Grisogono 2000; Pickett and Paduan 2003). Aircraft turbulence measurements have also been used to map the coastal near-surface wind stress field during several field experiments in the past (Enriquez and Friehe 1995; Rogers et al. 1998; Dorman et al. 2000; Ström et al. 2001; Brooks et al. 2003). Case studies from these datasets have shown that large positive wind stress curl occurs in the area of convex points or capes under strong northerly winds along the coast, which theoretically should increase the local upwelling. However, a systematic study of the effect of wind stress curl on local upwelling using observations has not been performed. Aircraft measurements with well designed flight patterns near the sea surface are capable of revealing the small-scale (≪100 km) spatial variation of the wind stress field. Thus, such measurements can be used to study the effects of wind stress curl on local upwelling if accurate estimates of the stress curl can be obtained through careful data processing.

A large volume of integrated observations were collected in the area of Monterey Bay, California, during the Autonomous Ocean Sampling Network (AOSN
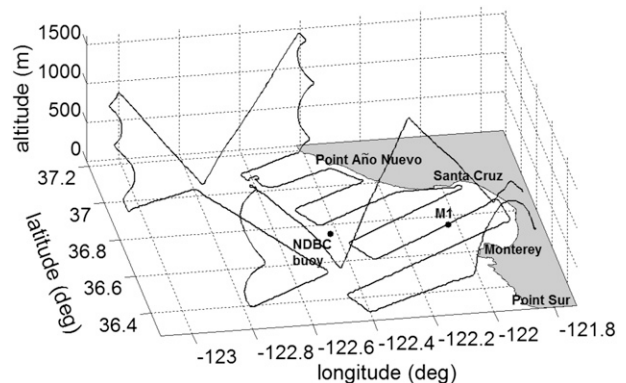

FIG. 1. A typical flight track of the Twin Otter in the area of Monterey Bay on 11 Aug 2003. Key points and cities mentioned in the text are labeled.

program in August 2000 and 2003 (Ramp et al. 2008). Using measurements from August 2000, Ramp et al. (2005) showed that the advection from upwelling centers to the north and south of the bay (Point Año Nuevo and Point Sur, respectively, shown in Fig. 1) may have a significant effect on SST inside the bay, while submesoscale variability of surface wind stress may play a role as well. However, aircraft measurements during August 2000 did not include high-rate sampling of turbulence; thus, the wind stress field was not available for the study of the significance of wind stress curl on local upwelling. In this work, aircraft turbulence measurements from the AOSN-II campaign are used with flights throughout a full year period (2003–04), and the measured SST field is compared to concurrent wind stress calculated using the eddy correlation method. Similar to other areas along the California coast, the meteorological conditions in this area are rather complicated, as indicated by previous studies, including significant flow channeling effects (expansion fan) due to the coastal topography and the low depth of the atmospheric boundary layer, which is capped by a strong temperature inversion (Winant et al. 1988); thermal circulations between land and sea (Banta et al. 1993); coastally trapped wind reversals with propagating southerly surges (Rogers et al. 1998); as well as frequent stratocumulus clouds during summer (Brost et al. 1982). Thus, wind and turbulence are characterized by significant small-scale spatial variability that results in large values of wind stress curl and probably local SST fluctuation. This small-scale variability can be resolved by carefully designed flight patterns.

In the following sections, we will first present the details of aircraft measurements and data processing together with error analyses on the results of surface stress and stress curl. Through this effort, we will demonstrate that aircraft measurements are capable of providing small-scale wind stress curl with sufficient accuracy when the

sampling flight pattern and data processing algorithms are carefully selected. Next, we will show averaged key parameters under various large-scale wind conditions using measurements taken during each condition and, whenever possible, in nearly consecutive flight days so as to reduce the spatial variability and identify persistent flow characteristics. The connection between SST field and advection by surface currents is verified using high-frequency (HF) radar data. A more in-depth study on a day with significant channeling effect and large wind stress curl is also presented to show the significance of wind stress curl on coastal upwelling during similar scenarios. Finally, the systematic occurrence of very low wind speeds, turbulence, and wind stress inside Monterey Bay is explained using aircraft soundings and near-surface measurements.

2. Measurements and data processing

a. Data and calculations of turbulence quantities

During the AOSN-II project, 40 flights were carried out in the area of Monterey Bay with the Twin Otter research aircraft operated by the Center for Interdisciplinary Remotely Piloted Aircraft Study (CIRPAS) of the Naval Postgraduate School (NPS) between January 2003 and February 2004 with an intensive observational period (IOP) during August 2003. Figure 1 shows a typical flight pattern that usually includes a low-level "lawn mowing" pattern close to the coastline, slant-path and spiral soundings at the northern and southern ends of the flight track, and a long leg parallel to the coastline at an altitude of 35 m in the offshore region. The "lawn-mower" pattern is done for near-surface sampling close to the coast. Results from these measurement patterns are of most interest in this paper. We note that the 50-m isobath—inshore of which the oceanic Ekman layer begins to occupy a significant fraction of the water depth and cross-shelf Ekman transport is reduced (Lentz 2001; Kirincich et al. 2005)—is within 10 km at most from the shoreline and only a small part of the flight pattern was within that distance from the shore (mostly legs along the shoreline). Thirty-three AOSN-II flights included the dense lawn-mowing flight pattern at 30–40 m above the sea surface as well as soundings at the northern and southern parts of the measurement area (Fig. 1) at an average airspeed of 55 m s^{-1}. Data from these flights were used to examine the horizontal distribution of various meteorological quantities as well as SST from an infrared radiometric thermometer. Additional measurements used in this paper include sea surface current from the local Coastal Ocean Dynamics Application Radar (CODAR) HF radar network (Paduan and Rosenfeld

1996) and ocean profiles from the Monterey Bay Aquarium Research Institute (MBARI) moorings.

Atmospheric turbulence measurements (10 Hz) were obtained with a radome probe combined with fast GPS attitude angle measurements for high-rate measurements of wind components, temperature, and water vapor (Kalogiros and Wang 2002a,b). Turbulent fluxes were calculated with the eddy correlation method using a horizontal averaging length of 5 km. Spectral analysis showed that this averaging length is sufficient and includes all of the energy containing scales when sampling is made along the crosswind direction. However, a significantly longer averaging length is needed in the case of along-wind sampling owing to the presence of longitudinal rolls in the atmospheric boundary layer that extend their effects to near the sea surface (Kalogiros and Wang 2011; Kalogiros et al. 2006). In the typical flight pattern (Fig. 1) most near-surface data were obtained with crosswind sampling since the most frequent wind directions were from the north or south directions along the shore. With the presence of longitudinal rolls, the spectral energy of momentum flux (wind stress) from crosswind sampling is shifted to high frequencies with a peak wavelength at ~150 m under the usually nonstable (unstable and near neutral) atmospheric conditions outside the areas with strong upwelling. Thus, the integral scale for momentum was small enough to permit four weakly correlated estimates of momentum flux within 5 km using overlapping segments. Despite the small turbulence integral scale, an averaging length of 5 km was used instead of a smaller one so as to keep the random error low in the estimation of turbulence quantities.

Wind stress curl is estimated using

$$\nabla \times \boldsymbol{\tau} = \frac{\partial \tau_y}{\partial x} - \frac{\partial \tau_x}{\partial y}, \tag{1}$$

where x and y are the east and north directions, respectively. The Ekman pumping velocity w_p is proportional to wind stress curl (Kraus and Businger 1994):

$$w_p = \frac{1}{\rho f} \nabla \times \boldsymbol{\tau}, \tag{2}$$

where ρ is the mean density of seawater and f the Coriolis parameter. The estimates of stress components τ_x and τ_y are first interpolated linearly onto a regular grid in the area of measurements with 5-km resolution. A 15 km × 15 km area averaging is also applied before calculating the required gradients of stress components using the centered difference scheme. This way a smooth variation of wind stress curl is estimated that retains the variations at scales larger than 15 km and with reasonable

accuracy, as discussed below. In section 2c, the effect of time variation of the wind field on the stress curl estimates will be discussed.

b. Error analysis

Errors in the estimates of turbulent fluxes include measurement errors, which propagate to the flux esti-mations, and various sampling errors. Sampling errors include systematic (bias) and random error due to finite averaging length and systematic loss of fluxes from high frequency variations due to limited sampling frequency. Since measurements were made at about 35 m MSL, errors may also be introduced because of the presence of vertical flux divergence when the fluxes at the measure-ment level are used instead of the actual surface fluxes.

The systematic sampling errors can be reduced using proper sampling parameters or corrected through post-processing efforts. As mentioned above, the averaging length of 5 km was sufficient to include all significant contributions of turbulence from energy containing eddies for crosswind sampling. This was also confirmed by the very small flux bias that was estimated according to Rannik and Vesala (1999). Assuming an inertial sub-range behavior at high spectral frequencies, flux loss due to low-pass filtering at Nyquist frequency (half the sam-pling frequency of 10 Hz) can be estimated. In the case of momentum flux, it was found that the flux loss is only 1% under the most frequently observed nonstable atmo-spherics conditions. Very rarely, the flux loss reaches 10% when the stability parameter z/L, where z is the measurement altitude and L the Monin–Obukhov length, reaches a value of 2.

Flux divergence correction for reduction of fluxes to surface can be significant for measurements made at 35 m above the sea surface. The flux profiles used for esti-mating the errors introduced by flux divergence were obtained from the slant-path sounding in the segments of ascent or descent soundings of a sawtooth pattern as shown in Fig. 1. For this purpose, the averaging length used to calculate fluxes is 1500 m along the slant path during which the altitude change is approximately 70 m. Composite profiles were constructed by normalizing the fluxes (horizontal axis) with the extrapolated surface fluxes and normalizing the altitude (vertical axis) using the boundary layer depth. Two groups of flux profiles were identified from the soundings of AOSN-II. One was characterized by a well-mixed linear flux profile up to the top of the atmospheric boundary layer at Z_i (boundary layer depth determined as the base of the strong temperature inversion capping the boundary layer). The other group of profiles, which was the most frequently observed case in AOSN-II, showed a well-mixed layer only up to about half the boundary layer
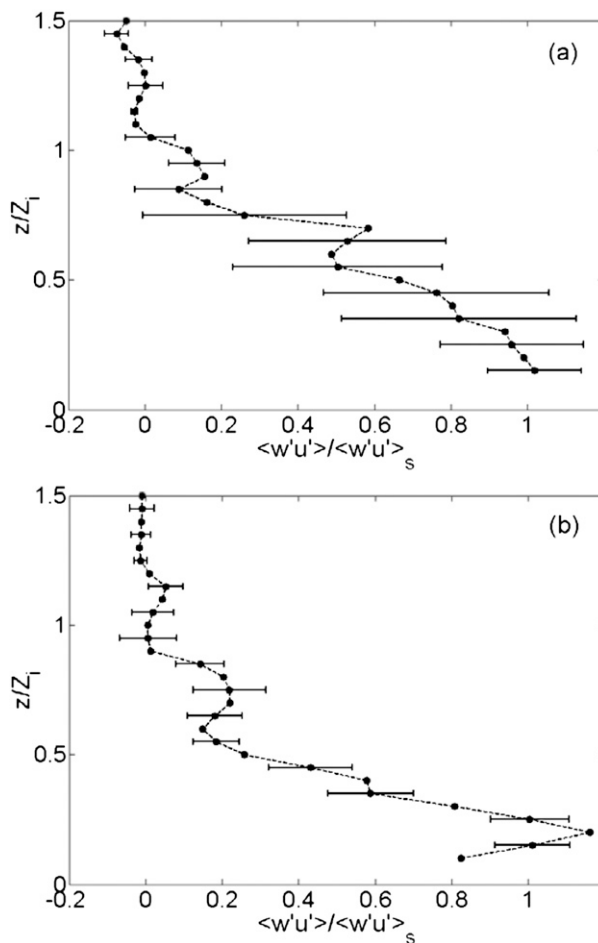

FIG. 2. Composite profiles and low-level momentum flux in the along-wind direction $(\overline{w'u'})$ for (a) well-mixed unstable and (b) incompletely mixed neutral atmospheric boundary layers. Stan-dard deviation of the mean is indicated by the horizontal bar on every other altitude level. The vertical axes are normalized with the boundary layer depth Z_i.

depth. This is due to the presence of stratocumulus clouds in the upper part of the boundary layer, which usually covers the measurement area at night and dur-ing early morning. Decoupling occurs frequently in the stratocumulus-topped boundary layers where the surface-based layer is generally well mixed (Betts 1990). For momentum flux under unstable and neutral near-surface conditions (Fig. 2), both profile types are characterized by small or nonsystematic flux divergence at the lowest levels. Thus, no correction was attempted for the dataset presented in this study. This choice was also supported by the fact that on average the drag coefficient estimated from the flux measurements agreed with a bulk param-eterization of the drag coefficient for wind speed values higher than 3 m s^{-1} and nonstable atmospheric condi-tions (Kalogiros and Wang 2011).

The random sampling error due to the stochastic nature of turbulence was estimated based on the spectral method described by Rannik and Vesala (1999) and a similar correlation method described by Finkelstein and Sims (2001). For wind stress this error was about 0.035 N m^{-2} or 25% on average for the dataset used in this study. The method to estimate the measurement errors of wind speed components from raw air pressure and attitude angles measurements is described in Buzorius et al. (2006). The random error for all three wind components was found to be about 0.1 m s^{-1}. The bias measurement error due to calibration increased the total error by 0.05 m s^{-1}. This bias error does not affect the results here because only fluctuations of wind components are used in flux estimation (variations at scales larger than the averaging length are removed). The random error propagates to the flux estimation as described by Enriquez and Friehe (1995). This error is inversely proportional to $\sqrt{N}$, where N is the number of data points used for calculating the flux. For wind stress, this error was relatively small, about 0.005 N m^{-2} on average. Thus, the total random error of wind stress is mainly due to the sampling error.

The propagation of wind stress error σ_τ to the wind stress curl gives an error $\sigma_{(\nabla \times \tau)} = 4\sigma_\tau/\Delta r$ (Enriquez and Friehe 1995), where $\Delta r = 10$ km is the distance between points used to estimate the gradients of stress components using a centered difference scheme. However, it should be noted that the error in wind stress is reduced significantly because of the smoothing of the stress field using the 15 km $\times$ 15 km area averaging before obtaining the gradients. As described earlier, there are four independent stress estimates in every 5 km of measurements, which gives a total of about 12^2 independent data points of stress in this averaging scheme. However, depending on the flight pattern, measurements may not cover all grid points of the 15 km $\times$ 15 km averaging area. Assuming f the percentage of measurement coverage (ratio of the number of grids with measurements to the total number of grids), the total number of measurements in one average area is hence $f \times 12^2$. The average wind stress curl error is estimated to be about 0.15 N m^{-2} (100 km)$^{-1}$ for $f = 50\%$ but may reach 0.25 N m^{-2} (100 km)$^{-1}$ for area coverage of 25%. For most of the AOSN-II data, f is found to be 50% or more. The reduction of error in the stress curl is mainly achieved after adequate smoothing of the stress field at the cost of losing spatial resolution and systematically smoothing out extreme characteristics (i.e., small scales) of the wind stress curl field. Figure 3 shows an example of the spatial distribution of the error of wind stress curl. In most of the experimental area the error of wind stress curl is well below its estimated value [absolute relative
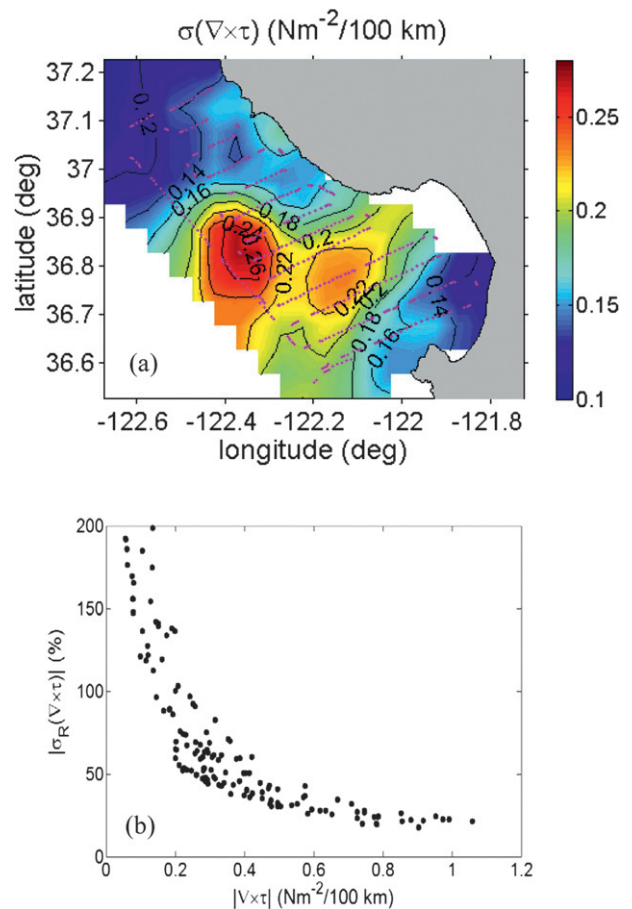

FIG. 3. (a) Total standard error σ and (b) absolute relative error σ_R of the calculated wind stress curl on 13 Jul 2003.

error less than 100% for stress curl above 0.2 N m^{-2} (100 km)$^{-1}$]; thus, these estimations are statistically different from zero. This is also supported by the fact that the estimated wind stress curl showed reasonable non-random spatial variation in the measurement region. Generally, even though the curl error is not low, it permits the identification of positive peaks in curl field where the value of curl is higher than about 0.2 N m^{-2} (100 km)$^{-1}$. The relative error (mostly random) of curl in areas with high stress curl goes to 20% and in areas with lower curl values is too high (above 100%), but these areas are of less interest in this study.

c. Nonstationary effect on the estimation of wind stress curl

The inability to separate spatial from temporal changes is an inherent shortcoming of all aircraft measurements. Some researchers (Vickers and Mahrt 1997) use the technique of performing repeated measurements over the same areas at different times to detect nonstationary effects. However, in our case there was no flight time left

to repeat the flight pattern. As most of our measurements took place in the morning, local nonstationarity of the wind field associated with the evolution of sea-breeze circulation (Banta et al. 1993) is a possible cause of error in our stress curl estimates. Wind measurements from the M1 buoy located in the center of the bay (Fig. 1) show a 1.5 m s^{-1} per hour increase of wind speed during the morning, which is mainly an increment of the onshore wind component. On the other hand, wind data from the National Data Buoy Center (NDBC) buoy 46042, located just offshore of Monterey Bay, usually shows smaller wind speed and direction variations during the flight (about 5 h). Thus, the nonstationarity problem affects mostly the nearshore part of the flight where a sea-breeze cell exists. This section provides an evaluation of this type of error.

Although a typical flight took about four hours, the stress curl is estimated using the near-surface lawn-mowing pattern close to the coast. For a typical flight, as that shown in Fig. 1, the near-surface lawn-mowing pattern is normally completed within a time window of about 2 h with relatively long legs cross-shore and shorter ones parallel to the coast (Fig. 1). Hence, the error in consideration is the result of the evolving wind field within the 2-h time window. Usually the lawn-mowing pattern consists of eight cross-coastline legs (cross legs). Thus, the time difference between adjacent cross legs is about 15 min. We mentioned in section 2a that the estimates of stress components τ_x and τ_y were first interpolated linearly onto a regular grid in the area of measurements with a 5-km resolution. A 15 km × 15 km area averaging is then applied before calculating the required gradients of stress components using the centered difference scheme on the 5-km resolution grid. We note also that the distance between cross-shore legs is also about 15 km. Thus, the measured stresses in the adjacent points in the y direction (parallel to the average coastline) are apart in time by approximately 15 min. In the cross-shore x direction, the adjacent points of measurements are a lot closer (5-km averaging length using overlapping segments). We therefore need to examine the effect of the nonstationary wind field on spatial differences within 15 min for estimating the error in the stress curl at a single point.

Using a simple bulk estimate of wind stress from wind speed (square law dependence) and drag coefficient, it can be estimated that for a typical morning evolution of the sea-breeze circulation, with evolving wind speed of 1.5 m s^{-1} per hour, there is a 10% increase of wind stress within a 15-min time period. This is a bias error, and its magnitude is small compared to the random error averaged at 25% (section 2b). This error will propagate to wind stress differences (i.e., wind stress curl), but

similarly it will be smaller [0.06 N m^{-2} (100 km)$^{-1}$ for 50% measurement coverage] than its random error estimated in section 2b.

We should note that the above estimation of an additional error in the calculation of wind stress curl due to the nonstationary wind field is an upper limit. This is because stress curl is defined as the difference between the y gradient of the τ_x stress component and the x gradient of the τ_y stress component [in Eq. (1) we may define x axis in the cross-shore direction and y axis in the parallel to shore direction]. The nonstationary effect is mainly caused by the sea breeze, which will mostly change the wind stress component normal to the coast (the x component) with a spatial gradient in the same direction. This was confirmed in one of our observed case (4 August 2003) when the sea breeze dominated the wind field in a low background wind condition. We compared the difference of wind and wind stress components at exactly the same flight segment at the beginning and at the end of the flight and found an apparent difference in the x component only. Thus, only τ_x will be affected, which reduces to half the total error of wind stress curl due to nonstationary wind field compared to the case that τ_y is affected as well. In addition, in the sea-breeze case the x gradient of τ_x is the dominant component compared to the y gradient, the latter being the one in calculating the wind stress curl, Eq. (1). This means that the actual error of wind stress curl is even smaller than the above estimation.

We further note that the above error analyses are for the stress curl at one single point. The stress curl distribution in the measurement region, however, was calculated from measurements within a 2-h period and may be distorted by the time evolution of the wind field. It is most accurate to say that the estimated spatial distribution is not a snapshot but a composite map within a time period of 2 h.

3. Results

The AOSN-II measurements were made under a variety of large-scale wind conditions that can be generalized into four basic categories based on the mean wind direction. Table 1 summarizes the wind speed and direction of each category as well as a few subcategories frequently observed during the 33 flights used in this study. The basic categories are defined based on average wind direction (nearly along or across the average California coastline direction of 315°). The subcategories are identified based on specific characteristics of the atmospheric flow such as wind acceleration at the northern part of Monterey Bay with possible expansion fan or southerly surge south of the bay. The typical wind conditions at the coast, especially during summer,

TABLE 1. Area-averaged wind speed U and direction (Dir) for each category of near–sea surface atmospheric flow in the measurement region.

Flow category	No. of cases	U (m s^{-1})	Dir
Northern wind	21	2.0–17.1	301°–360°
Acceleration	11	3.3–15.0	303°–350°
Expansion fan	3	10.3–15.0	317°–334°
Southerly surge	3	2.0–3.7	301°–360°
Southern	4	4.9–16.7	152°–154°
Eastern offshore	4	4.2–5.2	28°–98°
Western onshore	4	2.3–5.7	230°–269°
Southerly surge	1	5.5	238°

are north-northwesterly wind intensifying offshore because of the persistent high pressure system over the eastern Pacific Ocean. Significant channeling effects are observed when average wind speed is high (values greater than 10 m s^{-1}) and the wind direction is along the coastline. Southerly surges only occur in a small part of the measurements area and, thus, were incompletely sampled. Southerly wind directions are observed in the summer during short breaks of the dominant northerly wind conditions. Easterly offshore flow was observed

during the wintertime, bringing the cold air from inland. The cases of westerly wind occur on days with local thermal circulation (sea breeze) when the synoptic scale wind is weak.

Since we intend to study the relationship between stress curl and coastal upwelling, the coastal upwelling zone is of particular interest. Thus, we focus on measurements from the coastal upwelling zone defined by the baroclinic oceanic Rossby radius of deformation, which is about 20 km from the coastline (Pickett and Paduan 2003) and where most of the upwelling is expected to take place. Figure 4 shows the variation of 5-km averaged values of the near-surface wind, SST, wind stress, and wind stress curl as a function of local wind direction (where the wind is coming from) using measurements within the upwelling zone from all 33 Twin Otter flights.

The SST in Fig. 4 is represented as a difference between the SSTs far offshore and near shore, which we refer to as SST depression (dSST). The same approach was used by Tjernström and Grisogono (2000) to study SST changes and correlation with wind stress curl. Ideally, the local change in SST is a better indicator of upwelling than dSST. However, the local change of SST is
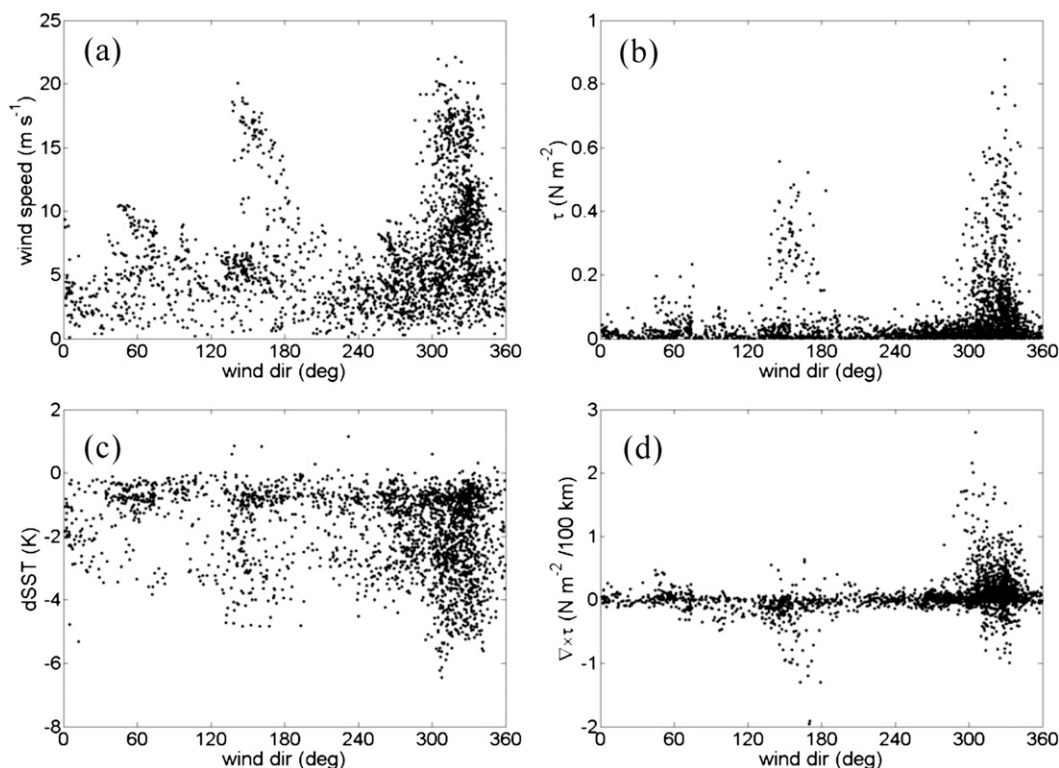

FIG. 4. Variations of (a) wind speed, (b) wind stress τ, (c) SST depression dSST, and (d) wind stress curl $\nabla \times \boldsymbol{\tau}$ as a function of wind direction (where the wind is coming from). Data shown were estimated from 5-km legs at about 35 m MSL in the coastal upwelling zone within 20 km offshore from the average coastline.

very difficult to estimate owing to significant spatial variations and the time lag of the ocean response in addition to the lack of continued SST measurements that cover the region. As the focus of this research is on the coastal upwelling in response to wind and wind stress curl, use of the SST depression is more relevant and is justified as an attempt to remove background upwelling to reveal the local effect of wind stress curl on upwelling. We also recognize that in reality advection of SST and ocean response may complicate the interpretation of the results. Our results (Figs. 6, 7) show that the offshore SST field is relatively homogeneous, which is advantageous in the effort to reduce the uncertainty of SST depression. In this paper, we used the maximum instead of the average SST in the far-offshore region as the reference temperature so as to avoid, as much as possible, the effects of upwelling in the offshore region. We note that, in this paper, the term "cool" or "cold" SST is a relative term, so we mean SST lower than the reference or average SST in the area.

Figure 4 provides an overview of all the cases sampled during the 1-yr measurement period. Figure 4a shows the strongest wind for the most frequently observed northerly wind condition. The largest wind stress also occurred in this wind sector (Fig. 4b). Significant positive stress curl and relatively cool SST are also identified in the same wind sector (Figs. 4c,d). However, Fig. 4 shows a much more complicated picture than a simple scenario of the SST depression induced by positive stress curl. We found dSST under strong southerly winds and significant negative wind stress curl, which cannot be explained as a result of coastal upwelling. Note that Fig. 4 only includes data from the nearshore region within the Rossby radius of deformation. When measurements from farther offshore were included in the analysis (not shown), there was no correlation between SST and wind stress curl in any particular wind direction. However, the stress-curl-enhanced SST depression is, indeed, observed in certain northerly wind conditions in the coastal upwelling region, although other factors may affect the SST for other wind directions. This is further explained in the following sections that present the spatial distribution of the relevant quantities under different wind directions. For easy reference, Table 2 lists the date and time of all cases to be discussed in this section. Figure 5 shows time series of the far-offshore wind speed and direction in the IOP time period 1–25 August 2003, at the NDBC buoy. This time period covers most of the events discussed in the next section.

a. Typical flow patterns

North-northwesterly wind along the coast was the most frequently observed wind pattern during AOSN-II. Such

TABLE 2. Date and time of all cases discussed in the text.

Flow category	Date (2003)	Time (LST)
Northwesterly wind	10, 11, 13, and 15 Aug	0915–1230
Southerly wind	20, 21, and 22 Aug	0930–1300
Westerly wind	4 Aug	0947–1342
Easterly wind	16 Dec	1003–1419
Expansion fan	13 Jul	1239–1657

wind conditions prevailed between 6 and 19 August 2003. During that time period, four Twin Otter flights occurred on 10, 11, 13, and 15 August 2003 at about the same time of day (Table 2). Wind measurements from the nearby NDBC buoy (Fig. 5) show a quasi-steady wind flow between 6 and 19 August 2003, which is a typical summertime upwelling event. Therefore, all four days were under similar large-scale forcing. Figure 6 provides the spatial distribution of the various quantities averaged using the measurements from the four flights. This averaging procedure is necessary for several reasons. First, the ocean response to the atmospheric forcing is not instantaneous.
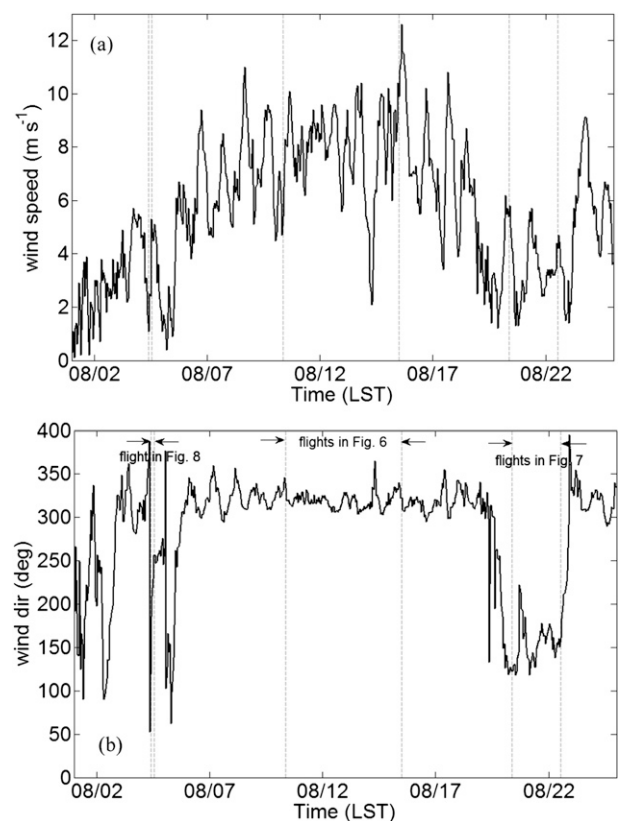

FIG. 5. Variation of wind speed and direction, between 1 and 25 Aug 2003, at NDBC buoy 46042 (36.75°N, 122.42°W). Dashed lines indicate the time periods of flights shown in Fig. 6 (0930 LST 10 Aug–1230 LST 15 Aug 2003), Fig. 7 (0930 LST 20 Aug–1300 LST 22 Aug 2003), and Fig. 8 (0947–1342 LST 4 Aug 2003).
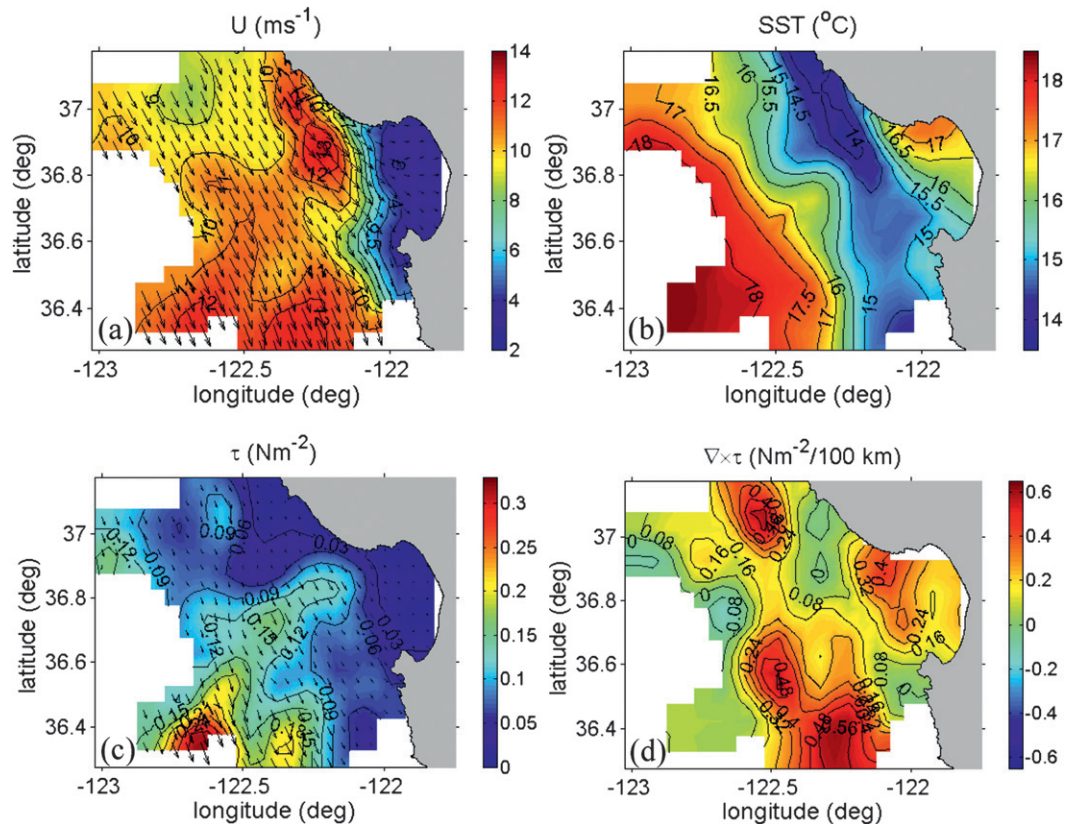
FIG. 6. Spatial distribution of (a) wind speed U, (b) SST, (c) wind stress τ, and (d) wind stress curl $\mathbf{V} \times \boldsymbol{\tau}$ estimated from aircraft legs at about 35 m MSL. The results were averaged from four aircraft flights on 10, 11, 13, and 15 Aug 2003 (from about 0915 to 1230 LST) under northerly wind conditions. All flights included in this figure used nearly the same flight pattern as that in Fig. 1.

There may be a delay up to several days in ocean response to wind forcing, depending on scale of the variation and the subsurface ocean temperature structure. For this reason, one should compare the field of wind forcing with a time-delayed SST field. However, the SST distribution measured in a consistent time sequence is not always available, especially with aircraft measurements. The averaged field, on the other hand, includes some information of the delayed ocean response. Second, this averaging process also allows us to retain the persistent features similar to averaging a simple time series of measurements. We should also emphasize that the flights used for averaging were made under similar wind conditions (Fig. 5) from nearly consecutive days and at about the same time of the day. The main features of the spatial distribution of various quantities from the individual flight are similar and the averaging process was able to retain the key persistent features and smooth out the small scale and high frequency variations, possibly due to statistical errors.

Figure 6a shows small variations (mostly in the range 10–12 m s^{-1}) in the wind field offshore, but the wind weakens significantly to 2 m s^{-1} within Monterey Bay. Moderate acceleration of the wind is observed in a limited region north of the bay. This acceleration is not significant enough to be considered a major wind speed maximum as in the case of supercritical flow and the expansion fan (Winant et al. 1988). Figure 6a shows a weaker wind inside the bay where the wind stress also decreases toward the coast in response to the reduction of wind speed. One possible reason for the weak wind inside the bay is sheltering from the coastal mountains. This effect will be discussed in detail in section 3d.

Although one can still identify an increase in wind stress associated with the high wind region at (36.9°N, −122.2°E), where the wind stress increased from near 0 to over 0.1 N m^{-2} in the along-wind direction, Fig. 6a shows that the maxima of the surface stress and the surface mean wind are not necessarily collocated particularly over the upwelling region of Point Año Nuevo to the north of the bay. This observation also holds for the fields of individual flights (not shown) as well as the 4-day average presented in Fig. 6. The increased atmospheric thermal stability is likely the reason for the

decreased wind stress here. Enriquez and Friehe (1997) found that stable stratification results in a negative feedback with significant impact on wind stress but very small effect on the SST field. Dorman et al. (2000) analyzed the spatial variation with much coarser resolution than our maps of surface stress and near-surface mean wind near Point Sur, south of Monterey, using aircraft measurements. Their results also showed that the main wind speed maximum may not be collocated with a corresponding wind stress maximum. Similar results were reported for a different location onth the California coast using aircraft data by Brooks (2001) and Ström et al. (2001) where on one measurement day the wind stress pattern was not well correlated with the wind speed field and a broad minimum of wind stress was attributed to the atmospheric stability effect due to a cold SST pool. It may be argued that, while turbulence adjusts quickly to changing atmospheric conditions, response of the wind speed field may not be as fast because advection terms can be significant in mean quantities equations but small in turbulent flux budgets (Brost et al. 1982). Thus, discrepancies between wind speed and wind stress fields may be observed in enhanced upwelling and expansion fan areas due to nonstationary and nonhomogeneity effects (Ström et al. 2001). In addition to surface thermal stability, sea state and, particularly, swell in the coastal area may have significant effects on wind stress at all wind speeds compared to the bulk estimates with no sea state effect (Geernaert et al. 1986; Donelan et al. 1993; Drennan et al. 2003). In low wind conditions, they may lead to high drag coefficients (i.e., wind stress). The direction of the wind stress may also deviate from that of the wind speed as a result of sea surface waves, particularly swell (Rieder et al. 1994; Grachev et al. 2003). In our measurements, the difference between wind and stress vector directions was within 20° on average, which is in the range reported in literature.

The spatial distribution of the wind stress curl (Fig. 6d) is complex owing to strong spatial variation of the wind stress field with small local extrema where the curl becomes zero (Fig. 6c). However, we can identify a general reduction of wind stress within the 20-km main upwelling zone and toward the coast under northerly winds, which leads to an effective average positive (cyclonic) wind stress curl of 0.4 N m^{-2} (100 km)$^{-1}$. This effective stress curl corresponds to the background Ekman transport, which in this event is comparable to the expected Ekman pumping due to the peaks of wind stress curl field [up to 0.6 N m^{-2} (100 km)$^{-1}$]. In areas of maximum positive wind stress curl, no depression of SST is observed, suggesting that the small-scale details of the stress curl pattern do not correlate with the SST pattern. On the contrary, the wind stress curl is smallest at the Point Año Nuevo area of cold SST and its southward extension. The maximum wind speed in this area suggests that SST advection from the upwelling center off Point Año Nuevo southward and in the mouth of Monterey Bay by surface currents could be a dominant factor, a result also shown by Ramp et al. (2005). This is supported by the SST field for each separate day of the event (not shown here), which shows an extension of the cold water pool from Point Año Nuevo to the south in addition to an intensification of this upwelling center (decrease of SST). Using the wind stress field from bulk parameterization (not shown here), which is quite similar to the wind speed field, the stress curl field becomes less complex as expected, but its correlation with cold SST pools does not improve. This can be understood by noting the position of the wind speed peak at the northern part of Monterey Bay relative to the cold SST pool under a northerly wind shown in Fig. 6. Positive stress curl values estimated from bulk parameterization are found on the east side of the wind speed peak toward the coast, whereas the cool SST area is located within the area of the wind speed peak and its west side. These results indicate that the depressed SST may not be collocated with positive wind stress curl as might be expected. This is not surprising though: other studies (Tjernström and Grisogono 2000) have shown that the effect of wind stress curl in the coastal zone may be masked by coastal upwelling due to northerly winds, which favor Ekman transport. Also, the effect of wind stress curl is spread over a broader area than the actual horizontal extent of nonzero curl due to the presence of the coastal boundary (Enriquez and Friehe 1995), and, thus, it is reduced (i.e., smoothed) compared to the classical far-offshore solution of Ekman pumping where upwelling rate is proportional to wind stress curl. Thus, it may be concluded that SST depressions due to Ekman transport or SST advection may be observed in areas with low positive wind stress curl. Results in Fig. 6 appear to indicate that, in some cases, the effect of upwelling due to Ekman pumping on SST may be of secondary importance relative to other processes such as SST advection by surface currents. We should also note that the gradients (small-scale variations) of sea surface currents can be significant and affect wind stress curl as well (Kraus and Businger 1994).

The flow characteristics for southerly wind conditions are illustrated in Fig. 7 using the average of observations from three successive southerly wind cases from 20 to 22 August 2003. These cases are usually breaks between the prevailing northerly winds during summer. Compared to the northerly wind condition in the previous case (Fig. 6), the southerly winds are weaker (note that different color scales are used for Figs. 6 and 7) and less variable. Reduced wind speed in the bay due to upstream
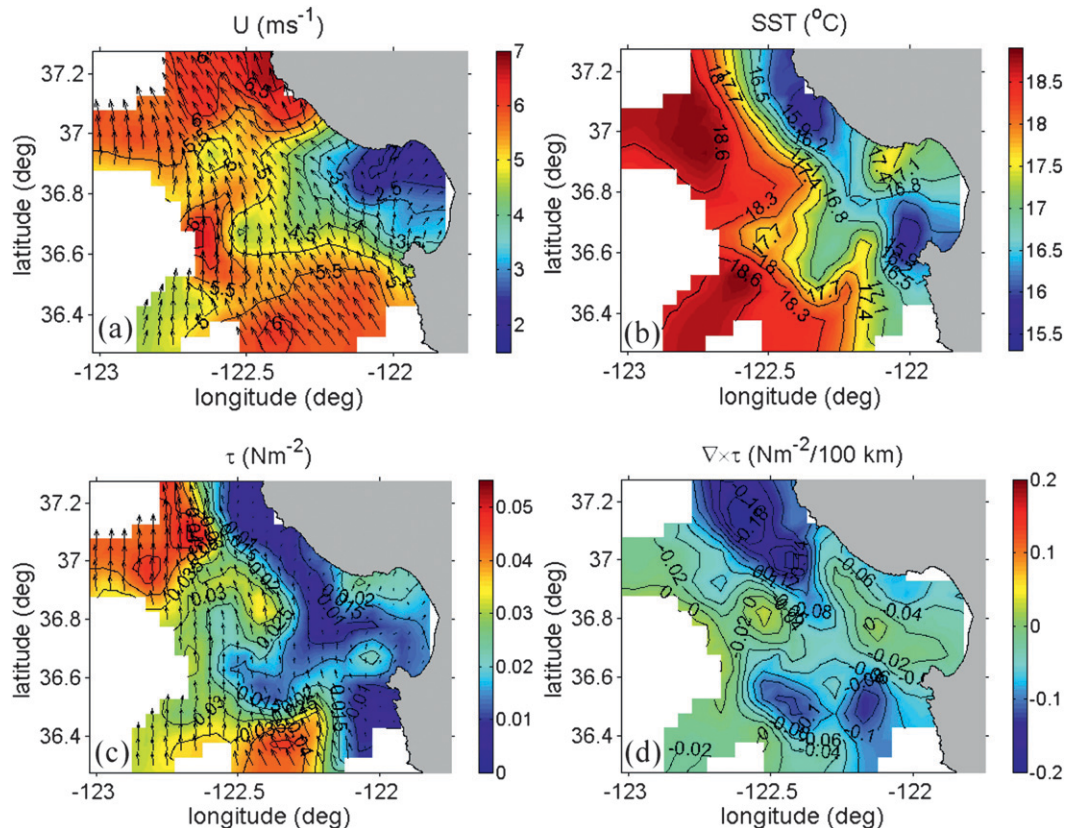
FIG. 7. As in Fig. 6 but for flights on 20, 21, and 22 Aug 2003 (from about 0930 to 1300 LST) under southerly wind conditions.

blocking from the Santa Cruz Mountains north of the bay is also seen in Fig. 7. The corresponding wind stress is also small in magnitude and shows more variability than wind speed, which is likely the result of weaker turbulence, mainly due to increased atmospheric stability over the region of low SST (southern air masses are warmer compared to northern ones too). Thus, there is a zone of low turbulence and low wind stress close to the shore. Under southerly winds, such a stress field should give negative wind stress curl, which is indeed observed in spite of the small magnitude compared to that in the northerly wind events. The cold SST center at Point Año Nuevo to the north of the bay is weaker, but still evident, despite that the southerly wind is not favorable for upwelling. The peak of negative wind stress curl and a cool SST center near Point Año Nuevo indicates that the potential warming of SST due to downwelling from the negative stress curl is not large enough to offset, within 3 days, the existing cool SST center previously generated during the northerly wind events. In addition, an area of low SST can be seen at the southern edge of the bay just offshore of the Monterey Peninsula. According to the SST fields from each of the three days of the event (not

shown here), this cold water patch progressively was warmed by 2 K and moved from a position out of the bay and to the south of it into the south part of the bay, which supports advection from the cold pool of the upwelling center near Point Sur by southerly winds. Point Sur, like Point Año Nuevo, is not an active upwelling center during this relaxation time period, but it was during the preceding upwelling event.

Figure 8 shows the spatial variations of the same variables as in Figs. 6 and 7 from a single flight (4 August 2003) with onshore winds (no such consecutive flights with similar flow characteristics were available). The wind speed is generally at its maximum at the mouth of the bay. According to measurements from the NDBC buoy, the background large-scale wind (Fig. 5) before the flight was weak, from the north, and turned to onshore flow during the flight. In addition to the changes in the large-scale background wind, the onset of the sea-breeze circulation (section 2c) also contributes to the temporal variation of the wind field, which also requires caution in interpreting the aircraft observation on this day. The sequence of the Twin Otter sampling was such that the center of the bay was sampled at the end of the
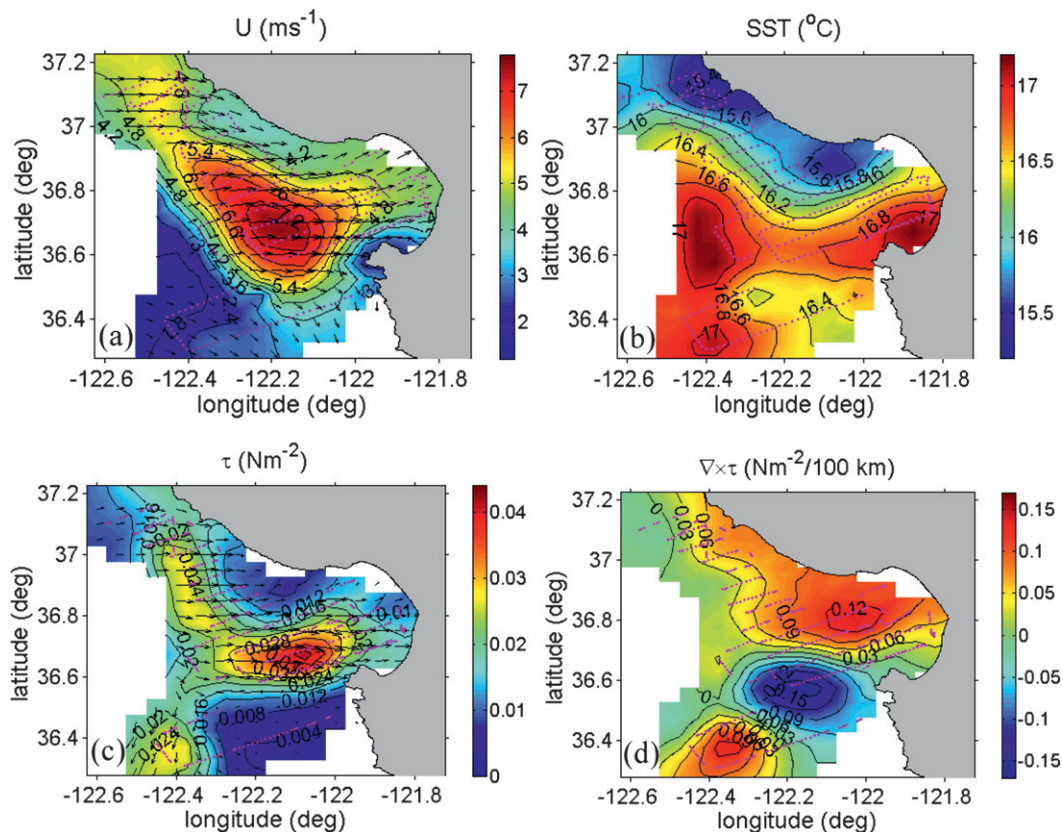
FIG. 8. As in Fig. 6 but for one flight from 0947 to 1342 LST 4 Aug 2003 with onshore winds. Purple points are the positions of the 5-km legs used for making the plots.

flight, and the observed flow pattern probably includes the effect of the sea breeze. Wind stress is small with a peak collocating with that of the wind speed. In contrast to the other flow patterns (Figs. 6, 7), there is an area of cold SST at the northeastern part of the bay. The wind stress curl in this case is generally small with values close to the error limit of the wind stress curl (section 2b). However, positive stress curl, which favors local upwelling (cool SST), consistently extends over the northern part of the bay.

The distribution of the surface current of this case (Fig. 9) can help us conclude if the characteristics of the SST field observed in Fig. 8 are associated with SST advection. We used the field of sea surface currents averaged in the 24-h time period before the flight to reduce the effect of the diurnal (tidal) variation of local currents and take into account the time delay associated with SST advection by sea surface currents. The amplitude of the semidiurnal mode M_2 constituent of tidal currents in the experimental area can reach 15 cm s^{-1}. Another mode with significant amplitude is the diurnal tidal constituent K_1, which is caused by wind variations such as the sea breeze (Paduan and Cook 1997). The M_2 mode, however,

is significant only close to the coastline, where the water depth is low (the 50-m isobath is within 10 km from the coastline as we mentioned in section 2a). Outside this area the amplitude of the M_2 mode is generally around 3–4 cm s^{-1}. Thus, only a small part of our data may be affected by this mode compared to the extended effect of the K_1 mode. In Fig. 9, a cyclonic circulation within the bay is evident in the average surface current with an offshore current at the northern part of the bay. Thus, the low SST in this area is not due to advection from the upwelling region off Point Año Nuevo in the north, which has also weakened, according to the SST field in Fig. 8. SST advection cannot explain the small SST maximum at the southern part of the bay either. This local maximum is probably the result of weak winds and near-surface heating by solar radiation.

The offshore flow pattern is illustrated using an example on 16 December 2003 (Fig. 10). This flow type usually occurs during wintertime and brings cold air from inland. According to the measurements at the NDBC buoy during 15–17 December 2003, the wind speed was moderate, in the range 1–8.5 m s^{-1}, coming from an easterly direction in the 0°–90° sector (not shown here).
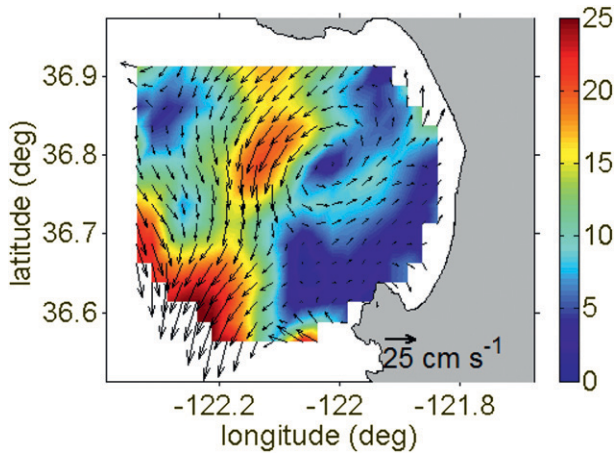
FIG. 9. Sea surface current from CODAR: results shown were averaged over the time period between 0900 LST 3 Aug and 0900 LST 4 Aug 2003 (i.e., the time period before and during the flight on 4 Aug 2003). The color filling denotes the magnitude of the current.

An internal boundary layer develops along the distance from the shoreline with a maximum wind speed and wind stress offshore at the mouth of Monterey Bay. Similar to the onshore event, there is a well-defined pattern of wind stress curl with, however, opposite sign and larger magnitude owing to the stronger wind and turbulence in the offshore wind condition. Thus, positive wind stress curl is found at the southern part of the bay. Colder SST relative to far-offshore values can be seen in the bay extending to the south, which is likely caused by both the stress-curl-induced upwelling and offshore advection by surface currents. These currents were caused by the offshore wind and stress and were observed in CODAR measurements in the 24-h time period before the flight (not shown here). Unlike the summer cases, there are no persistent wind conditions that favor upwelling along the coast; thus, the persistent cool strip of SST, particularly to the north of the bay, is no longer observed in Fig. 10.

b. Sea surface currents and SST advection

Based on the discussions in the previous section, we see indications that positive wind stress curl is correlated with local SST reduction when it extends coherently (i.e., systematically) over a significantly large area (order of scale larger than 20 km) and when background coastal upwelling (Ekman transport) is weak such as in the onshore and offshore wind conditions (Figs. 8, 10). This correlation is not evident for the northerly or the
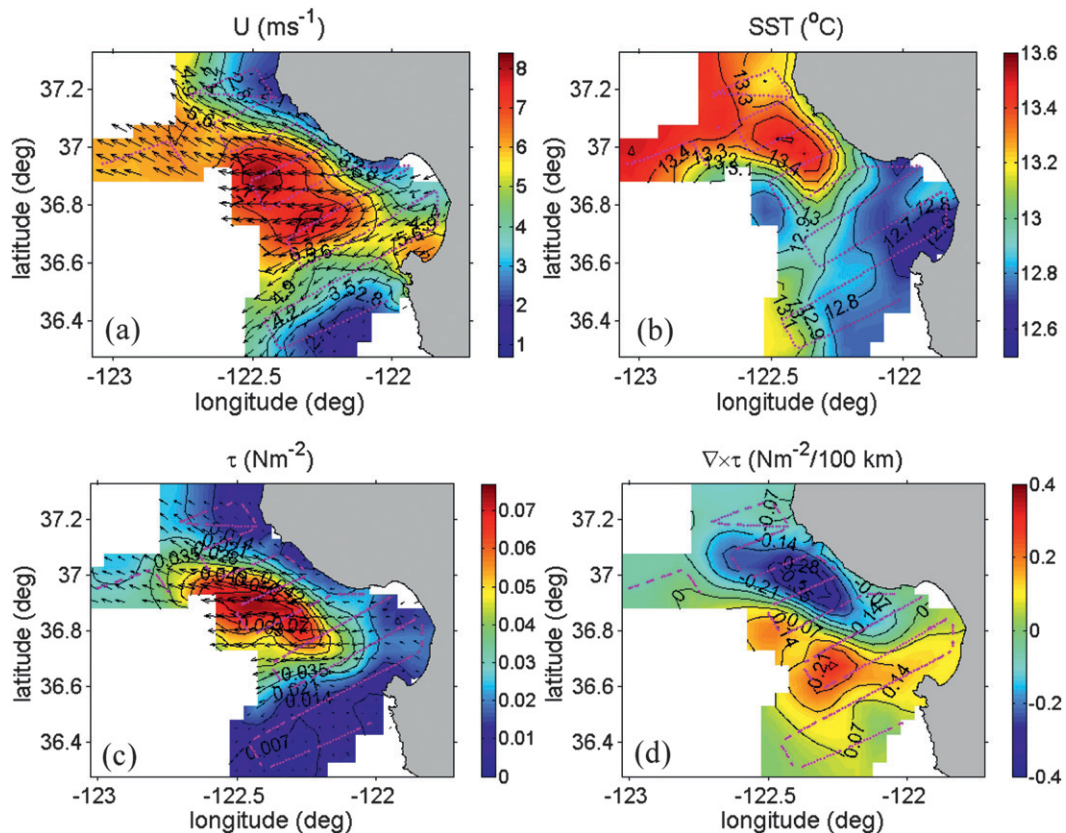

FIG. 10. As in Fig. 8 but for one flight from 1003 to 1419 LST 16 Dec 2003 with offshore winds.

southerly wind conditions. The stress curl was generally positive during the northerly wind event. However, near-zero values were observed in the area of strong coastal upwelling centers as at Point Año Nuevo, and positive values were observed within the bay with no SST depression. This discrepancy in the area of upwelling centers may be due to the dominance of offshore Ekman transport over Ekman pumping or the delay between wind forcing, upwelling, and cold SST. During the southerly wind event, the wind stress was generally low and negative wind stress curl was observed close to cold SST regions. In fact, in both northerly and southerly wind cases, the wind turbulence pattern was complex with significant small-scale variations and a reduced magnitude of turbulence in the areas of low SST due to stable thermal stratification in the atmospheric surface layer. Wind stress curl and the resultant upwelling is probably not a major factor in controlling the SST field in the Monterey Bay area under northerly and southerly wind conditions, but SST advection could be an important factor.

Figure 11a shows the correlation of SST depression (defined in the same way as that shown in Fig. 4) and alongshore current, defined as the component of sea surface current parallel to the average coastline direction. The surface currents are 4-h averages of CODAR measurements during each flight, for the same reasons as mentioned in the discussion of Fig. 9, and they are limited in the area of Monterey Bay (the area where they are available). We also separate the northerly wind conditions from other wind conditions. Although "other categories" does not show apparent correlation between the SST depression and the alongshore currents, the correlation is rather clear for the northerly wind conditions. This observation suggests the advection of colder SST from the upwelling area at the north of Monterey Bay to the center and the mouth of the bay. Significant scatter is seen for the remaining wind categories dominated by southerly wind conditions and weak surface currents. This component of sea surface current along the coastline is well correlated with the corresponding wind component (Fig. 11b), which implies the dominant role of the wind forcing on SST advection.

c. Local upwelling due to Ekman pumping

In the previous sections, we found that the positive wind stress curl and associated Ekman pumping usually does not lead to colder SST, which serves as an indicator of enhanced coastal upwelling in the experimental area of AOSN-II. In this section, we discuss an exception to that finding when lower SST due to the contribution of Ekman pumping can be clearly identified. This is a case with an expansion fan downwind of a coastal point with supercritical upwind conditions. This type of event at the
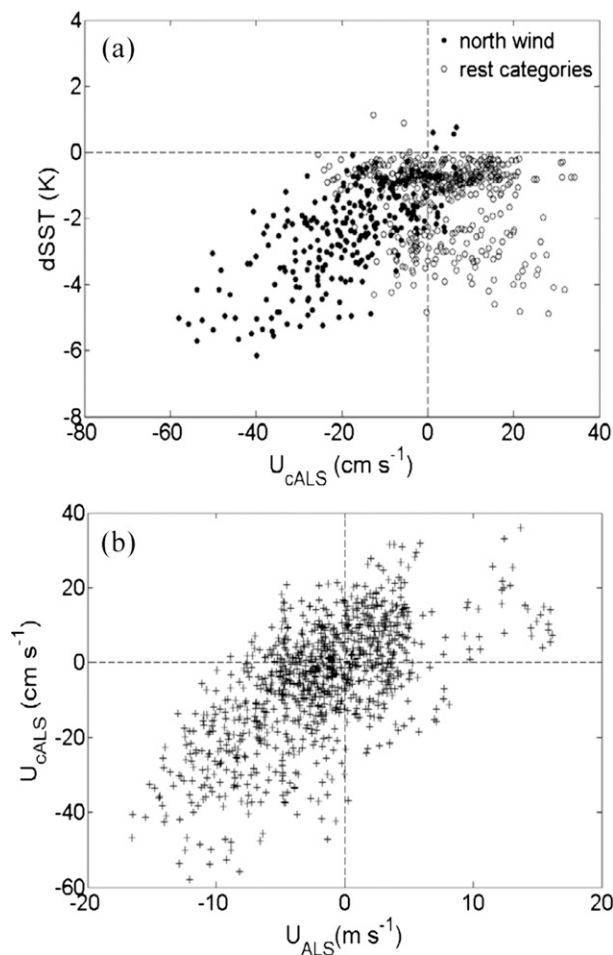

FIG. 11. (a) Correlation of the dSST at the center of Monterey Bay with the surface current component along the average direction of the coastline at ~315° U_{cALS} and (b) correlation of U_{cALS} with the corresponding surface wind speed component along the same direction U_{ALS}. Filled circles are from flights in northerly wind conditions with acceleration or expansion fan (see Table 1) and average wind speed above 5 m s^{-1}.

northern area of Monterey Bay is not frequent (Table 1), but, for other more significant points and capes along the California coast expansion fan events are common (Enriquez and Friehe 1995; Winant et al. 1988; Rogers et al. 1998; Dorman et al. 2000; Brooks et al. 2003). The case was observed from 1239 to 1657 LST 13 July 2003. Figures 12 and 13 present the horizontal distribution of various meteorological quantities from this case. Figure 12a shows a rapid acceleration of wind speed accompanied by wind direction change at the turn of the coastline at the north of Monterey Bay, characteristic of an expansion fan originating from Point Año Nuevo. Figures 13a,b show a region of warm near-surface air temperature and low surface pressure at the northern part of the bay, indicating a significant and fast reduction of
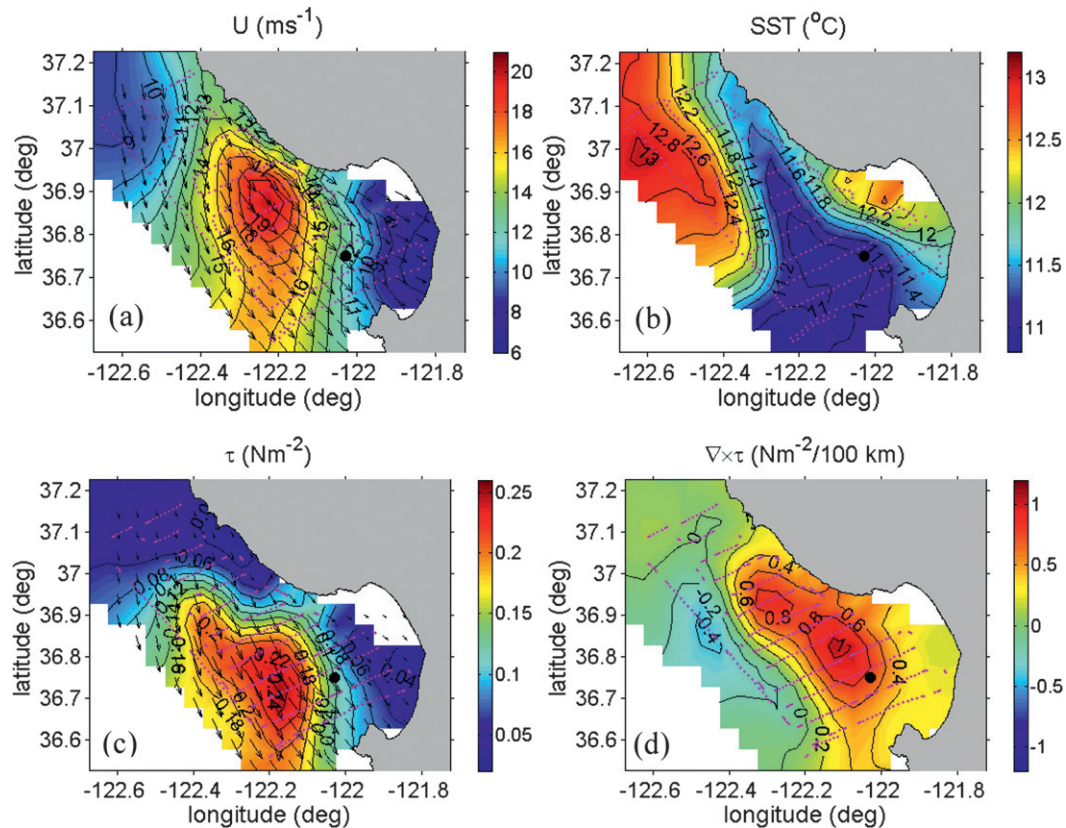
FIG. 12. As in Fig. 6 but for the flight from 1239 to 1657 LST 13 Jul 2003 with possible expansion fan to the north of Monterey Bay. The black filled circle shows the location of buoy M1.

boundary layer depth in this region. Using measurements from the aircraft soundings at the northern part of the flight track, the upwind Froude number was estimated using the average wind speed in the boundary layer, the height of the marine boundary layer defined as the base of the usually steep temperature inversion capping the marine boundary layer, and the difference of potential temperature between the top and the base of the capping temperature inversion. This method is similar to many others used in previous literature within a shallow water framework (Dorman et al. 2000). Whenever available, the sounding close to the coast at the northern part of the flight area (see flight pattern in Fig. 1) was used to estimate the above parameters. We note here that the term "upwind" refers to the conditions at the northern part of our experimental area before the local turn of the coastline. The estimated upwind Froude number was about 2.0, suggesting supercritical flow conditions. We note that, even in transcritical expansion fans, the Froude number becomes supercritical just before the turn, although it can be subcritical further upwind (Rogerson 1999). From the same set of soundings, it was also found that the boundary layer

height upwind of the bay was only 150 m and lowered to about 50 m in the center of the bay. Similar conditions were shown in Burk and Haack (2000) for the same area using a high-resolution mesoscale model. They documented a peak of wind speed at the same location and a hydraulic jump (shock) in the downwind direction.

The center of maximum wind stress is located slightly to the south of the peak wind speed (Fig. 12c). A well-defined center of the positive wind stress curl is also apparent with maximum stress curl exceeding 1 N m^{-2} (100 km)$^{-1}$ at the mouth of the bay. In contrast to the northerly wind event described in section 3a, wind stress (Fig. 12c) and turbulence (vertical velocity variance; Fig. 13d) peak at the area of the coldest SST (Fig. 12b) and increased atmospheric thermal stability, indicated by the significant negative heat flux center (Fig. 13c). These observations are clear evidence of an expansion fan to the north of the bay. Similar characteristics have been observed from aircraft measurements at other more significant capes and points along the California coast (Enriquez and Friehe 1995; Rogers et al. 1998; Dorman et al. 2000; Brooks et al. 2003).
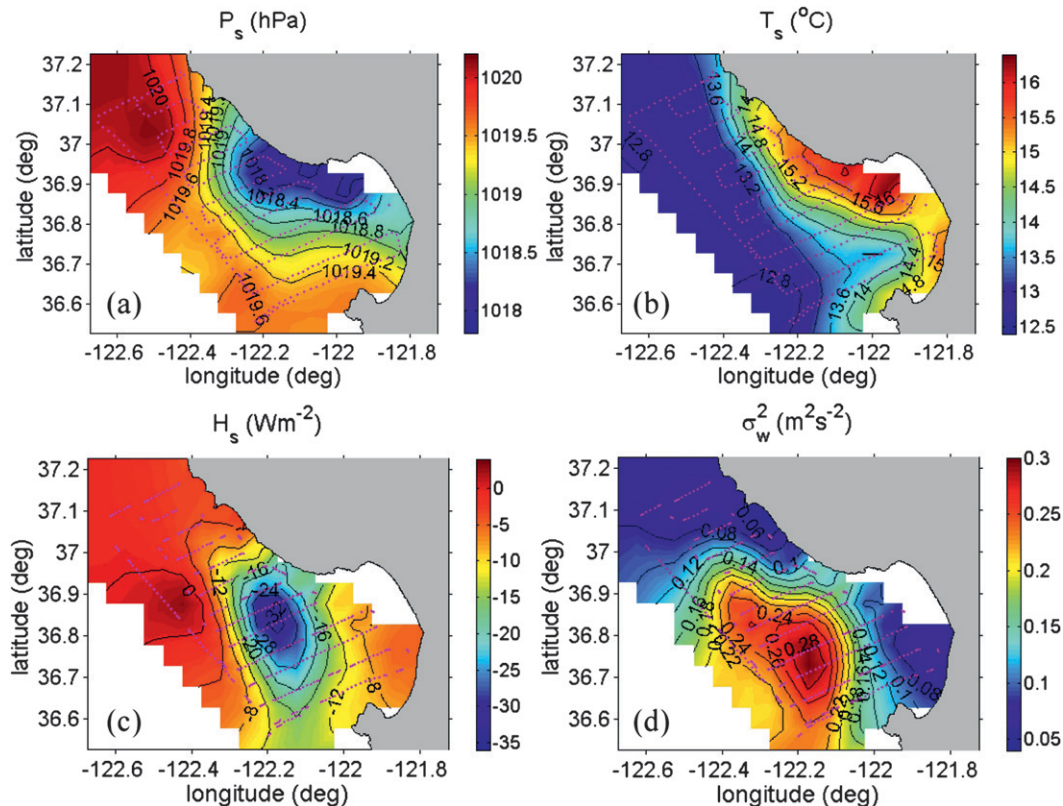
FIG. 13. As in Fig. 13 but for (a) sea level static air pressure P_s, (b) air temperature T_s, (c) turbulent sensible heat flux H_s, and (d) vertical velocity variance σ_w^2.

Measurements from the MBARI buoy (M1) located in the center of the bay (the black circle in Fig. 12) further support the findings from our aircraft measurements that the observed cooling of the upper ocean was a result of Ekman pumping. Figure 14 shows the wind speed, wind direction, and vertical profile of water temperature from buoy M1 covering also the periods before and after the aircraft measurements. Here, we clearly see the diurnal variation of the wind field, particularly on 12 and 13 July and less on 14 July. In particular, dominant northwesterly wind was seen on 12 July, a day before the aircraft measurements. For all three days, wind direction became almost steady in late morning (1000–1200 LST) when rapid acceleration of the northwesterly wind began. Peak wind speed was reached at approximately 1800 LST. The upper-ocean temperature also showed diurnal variations with the warmest SST and a surface layer depth (e.g., defined by the isotherm of 10 K, which shows a clear diurnal change) of several meters in the early afternoon. Rapid cooling of the upper 20 m of the ocean appears to start after 1200 LST, when the wind speed increased to more than 6 m s^{-1} and the flight on 13 July took place. It is possible that the peak positive stress curl was much reduced or absent earlier in the morning when the wind

speed was much lower. A delayed response (a couple of hours for the scale of this upwelling event) of the ocean to the wind forcing is also expected, as discussed earlier. Thus, we do not expect the time of peak wind speed and stress curl to coincide exactly with the time of minimum depth of the ocean surface layer. We also notice a generally decreasing trend of the depth (a couple of meters per day) of the ocean surface layer from day to day, caused by upwelling due to Ekman transport superimposed on a diurnal cycle with maximum upwelling rate just above 15 m day^{-1} due to the increase of wind speed and appearance of the peak of positive stress curl within each day. On 13 July 2003, the day when the aircraft observed the presence of the expansion fan, we see the shallowest ocean surface layer and the most significant cooling rate of the three days. The peak wind stress curl observed during the flight on that day (Fig. 12d) is 1.06 N m^{-2} (100 km)$^{-1}$ (i.e., upwelling due to Ekman pumping about 10.5 m day^{-1}) with an error of about 0.2 N m^{-2} (100 km)$^{-1}$ according to Fig. 3 for the same day. The SST field is warmer in the upwind region at Point Año Nuevo (Fig. 12b) than in the central area of the bay; thus, we can exclude SST advection as a cause of the upper-ocean cooling seen at he M1 buoy. The
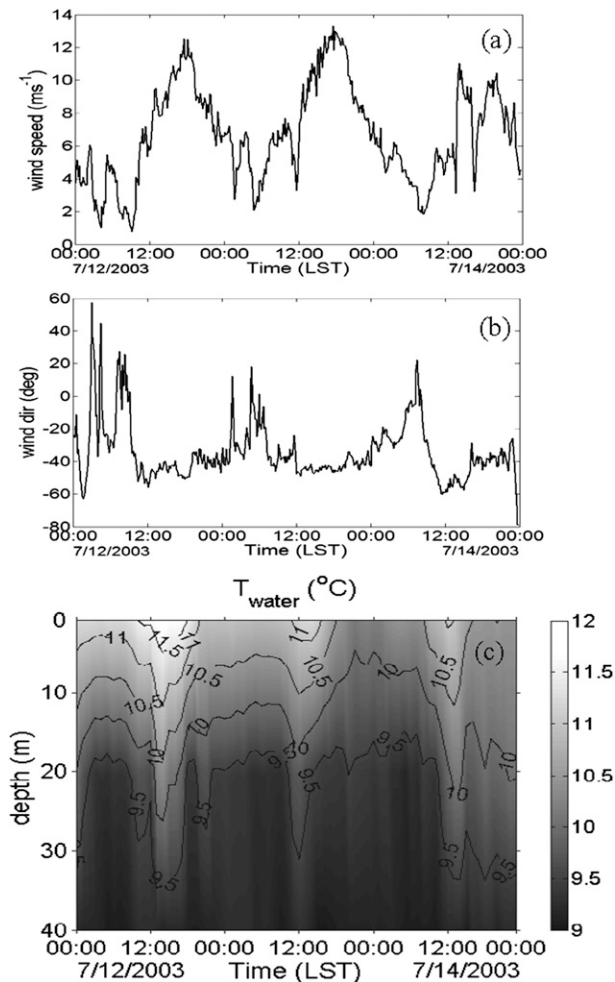
FIG. 14. Variation of wind speed and direction and vertical profiles of water temperature T_{water} between 12 and 14 Jul 2003 from buoy M1 (36.75°N, 122.03°W). Note that the range of wind direction is within the range −180° to 180° to avoid abrupt changes of wind direction. Aircraft measurements were made between 1239 and 1657 LST 13 Jul.

cooling has hence resulted from upwelling caused by the significant positive stress curl (Ekman pumping) at the mouth of Monterey Bay (Fig. 12d). This result is consistent with all other modeling and observational studies of the expansion fan off the California coast (Enriquez and Friehe 1995; Rogers et al. 1998; Dorman et al. 2000; Brooks et al. 2003).

d. Effects of topographic sheltering in Monterey Bay

Topography and coastline play a significant role in the spatial variations of the coastal meteorological and oceanic conditions. In this section, we focus on the area inside Monterey Bay to explore possible mechanisms that underscore the effects of wind stress curl on upwelling and SST distribution. As seen in section 3a,

under northerly wind conditions, low wind and turbulence in Monterey Bay with higher SST at the northern part of the bay were frequently observed. Winant and Dorman (1997) described similar conditions in the Southern California Bight of wind sheltering (shadowing) in the area off Santa Barbara using observations from ships and buoys. They attributed their observed phenomena to be the possible result of separated flow downwind of a supercritical flow (expansion fan) due to the significant turn (close to 90°) of the coast. The same explanation should hold for our observed cases as well. However, we find that sheltering appears to occur in all northerly wind events, despite the absence of an expansion fan in the flow. Below, we describe a case of wind sheltering without a corresponding expansion fan.

Figure 15 shows cross sections of the virtual potential temperature of air and wind speed upwind and in Monterey Bay on 17 March 2003. The upwind boundary layer was deep, at about 550 m (Fig. 15a). However, there is a significant lowering of boundary layer height in the bay to below 100 m (Fig. 15b), with a significant reduction in the wind speed and turbulence close to the surface (not shown). The significant drop in boundary layer height can be caused by the presence of an expansion fan (Dorman and Winant 2000) or lee wave sheltering even in the presence of an expansion fan (Tjernström 1999). Transcritical expansion fans are characterized by significant wind speed acceleration, which can be easily identified in the spatial distribution of the wind speed (e.g., the case shown in Fig. 12). However, wind speed acceleration was not observed in the flight shown in Fig. 15, where wind speed stayed at ~17 m s^{-1} near the surface around the coastal bend at the northern part of the bay with weaker wind within the bay (not shown). Thus, the expansion fan characteristics (wind speed acceleration along with boundary layer reduction) were not observed at the coastal bend at the northern part of the bay, even though the Froude number estimated from sounding data at the northern part of the flight area was slightly supercritical (above 1.0). A similar case was reported by Enriquez and Friehe (1995) under northerly wind conditions. This is due to the weak (about 2 K) strength of the temperature inversion at the top of the marine boundary layer and, thus, weak mesoscale pressure gradient corresponding to changes of boundary layer depth (Burk et al. 1999). Thus, the collapse of the boundary layer depth in the bay, in Fig. 15, is most likely a result of sheltering by the coastal topography. Figure 16 shows the connection of average near-surface wind speed with boundary layer height for all AOSN-II flights with available soundings from the sounding section of the flight starting at the open sea and ending in the bay (see Fig. 1). Trends can be identified at wind speeds
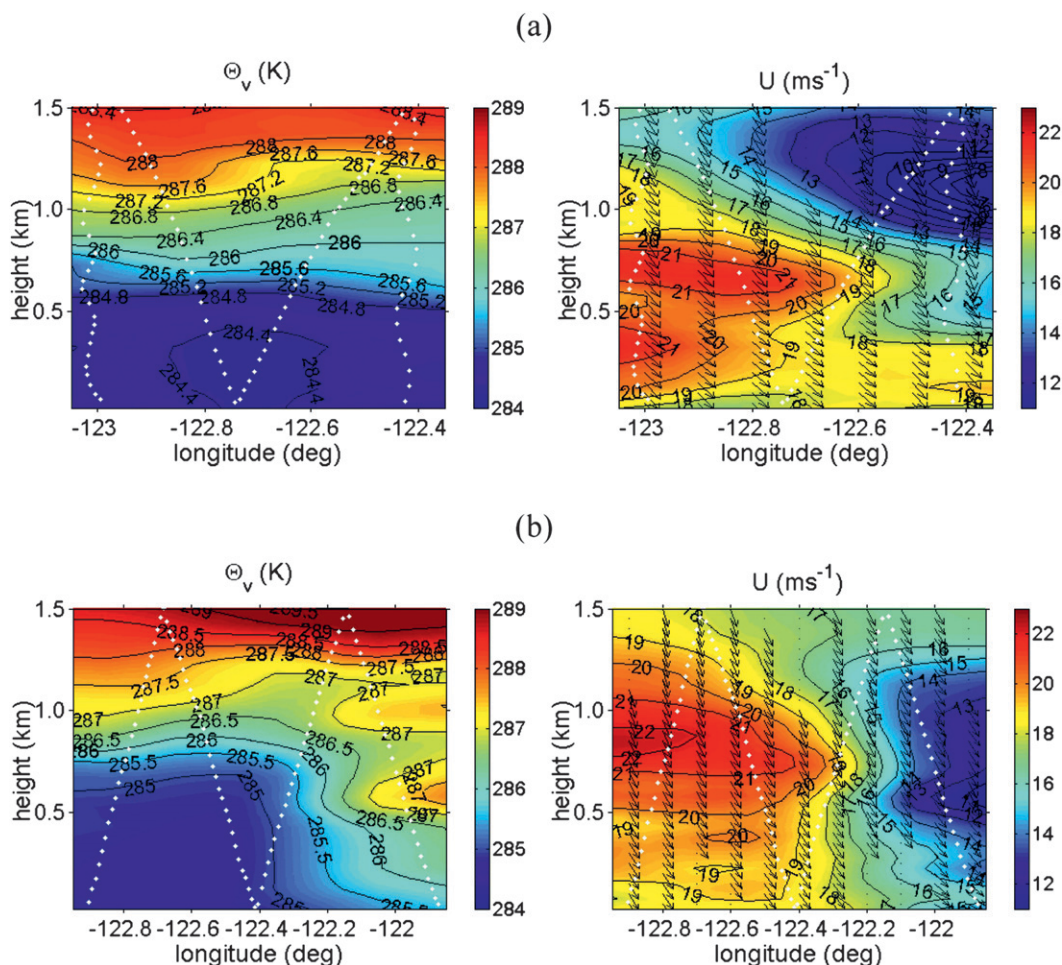
FIG. 15. Cross sections of virtual potential temperature Θ_v and wind speed U using the soundings (a) upwind (north) of and (b) into Monterey Bay (see the typical flight track in Fig. 1) on 17 Mar 2003. White dotted lines denote the flight tracks used to generate the plots.

above 5 m s^{-1}. Over the open ocean higher wind speed is combined with higher boundary layer thickness. On the other hand, the boundary layer in the bay stays around 100 m and decreases when the average wind speed exceeds about 10 m s^{-1}, which includes the high wind acceleration and expansion fan cases shown in Table 1. Thus, this additional reduction of boundary layer height in the bay is associated with channeled flow.

The reduction of turbulence and wind stress in the sheltered area generates positive (cyclonic) wind stress curl (see, e.g., Fig. 6 inside Monterey Bay for the northerly wind event). However, a warm SST center was observed at the northern part of the bay instead of any signs of cooling, as it is the expected result of the Ekman pumping from the positive wind stress curl. In the case of a southerly wind (Fig. 7), the generation of negative wind stress curl in the bay due to wind shadowing is

significantly smaller and vague. Ramp et al. (2005) and Graham and Largier (1997) also reported the frequent occurrence of such wind shadowing at the northern part of the bay and the associated warm SST patch that they attributed to heating processes such as absorption of solar radiation. In the shadowed area at the northern part of Monterey Bay the oceanic surface layer is shallow because of the weak winds. Graham and Largier (1997) estimated the local depth of the oceanic surface layer to about 7 m according to CTD observations. With this shallow surface layer and clear-sky conditions during the summer upwelling season, they estimated an average heating rate of surface water of ~0.5 K day^{-1}. However, in the shadowed area they estimated also a large residence time of about 8 days, possibly via water recirculation; thus, the sea surface temperature may increase eventually by 3–4 K owing to solar heating. The positive wind stress curl at the same area as in Fig. 6
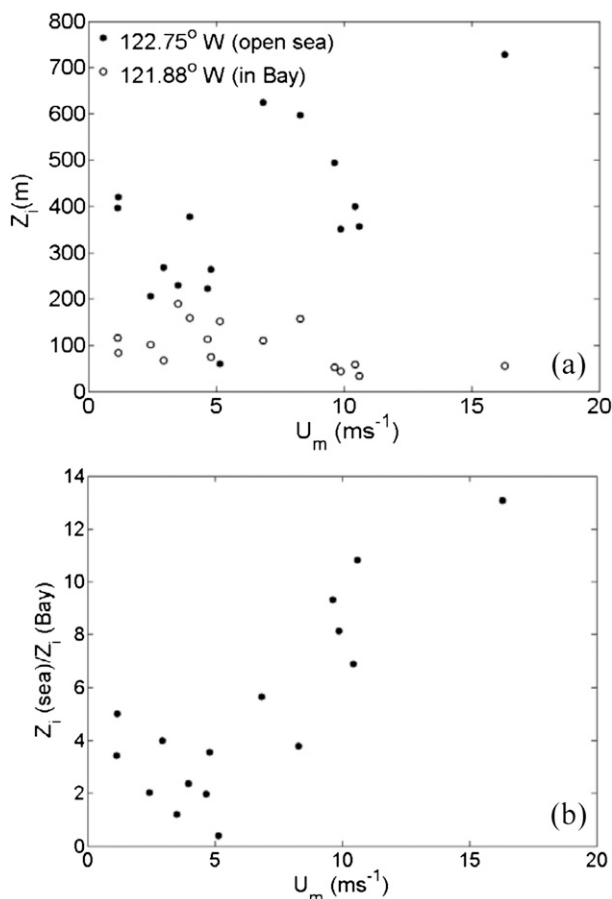
FIG. 16. Boundary layer depth Z_i and ratio at two almost fixed positions (at the offshore–open sea and in th Monterey Bay) from the sounding section of the flight starting at the open sea and ending in the bay (see Fig. 1) against aircraft-measured area-averaged near-surface wind speed U_m.

should produce upwelling and thus a local cooling of SST. This cooling is, however, not observed, because the heating of the oceanic surface layer by solar absorption may be too high (3–4 K, as mentioned above) and dominates the cooling by the weak local upwelling due to Ekman pumping in the area. The Ekman pumping velocity at the northern part of Monterey Bay is about 3 m day^{-1}, according to Fig. 6, and the water temperature gradient is probably about 1.5–2 K/20 m near the surface, as in Fig. 14. In addition, the intensity of upwelling due to wind stress curl is significantly reduced close to the coast compared to offshore Ekman pumping (Enriquez and Friehe 1995), as is the case of Fig. 6. The significance of solar heating on SST in northern Monterey Bay is illustrated well by satellite SST images and HF radar–derived currents in upwelling conditions, as presented in Plate 1 of Paduan and Rosenfeld (1996). The small offset between warm SST and positive stress curl peak (but still positive stress curl is estimated over

the whole area of warm SST) should not be critical for this qualitative conclusion of local dominance of radiation heating over Ekman pumping.

In conclusion, under the aforementioned atmospheric conditions both wind sheltering by the coastal mountains and flow channeling contribute to the shallow atmospheric boundary layer in the bay with associated weak turbulence (wind stress) and shallow oceanic surface layer. However, sheltering by local topography is more significant and occurs more frequently. Although there is significant positive stress curl observed at the same location, warm SST is found as a result of direct heating of the shallow surface layer by solar radiation. Thus, in addition to SST advection (section 3b), the heat balance at the sea surface can be a significant factor that obscures the effects of upwelling from Ekman pumping in areas of coastal wind sheltering.

4. Summary and conclusions

Turbulence measurements from a research aircraft during the 2003 AOSN-II campaign were used to study the effect of submesoscale wind stress curl on coastal upwelling through Ekman pumping in the area of Monterey Bay. The wind stress curl involves estimating the difference between spatial gradients of a turbulence quantity, for example, wind stress: it is therefore difficult to obtain with sufficient accuracy, especially at small scales. Our error analysis showed that wind stress curl can be estimated with an average error less than 0.2 N m^{-2} (100 km)$^{-1}$, using near-surface measurements from a carefully designed flight pattern as well as a refined data processing scheme. In particular, sufficient spatial smoothing was required to reduce the random error in the estimation. The accuracy of the wind stress curl obtained is adequate for analyzing the variations of wind stress curl at scales larger than 15 km.

No clear correlation was seen between SST depression and wind stress curl when all data from AOSN-II were used in the analysis. Thus, a detailed analysis of various events with different atmospheric conditions was performed. Although the wind stress curl is positive and large in magnitude under northerly wind conditions, the spatial variations of stress curl were not correlated in general with SST depression. This was attributed to the complex and noncoherent small-scale variations of wind stress curl due to the relatively uniform wind field with no significant peaks. The upwelling due to the relatively small peaks of wind stress curl (Ekman pumping) in the coastal zone may be reduced and spread over a broader area compared to far offshore or masked by coastal upwelling because of northerly winds (Ekman transport) on the same order of magnitude as the stress-curl-driven

upwelling. Thus, small-scale variations of wind stress curl may not correlate with SST pattern. The negative feedback of coastal upwelling on wind stress through atmospheric thermal stability also contributes to the weak correlation. Similar behavior was observed under southerly winds when wind stress curl was small and negative. In these events, SST advection from strong upwelling regions at the north and south of Monterey Bay are more significant for the formation of SST variations in the central area and at the mouth of the bay. On the other hand, when the wind stress curl field is characterized by coherent structures (significant positive values extending over scales larger than 20 km) and Ekman transport is weak (as, e.g., in the case of onshore or offshore wind and stress conditions), a clear connection of wind stress curl with locally enhanced SST change was observed. The most evident effect of wind stress curl on coastal upwelling was seen under northerly winds when an expansion fan with significant wind speed acceleration and a peak of very high wind stress and wind stress curl occurred at the mouth of Monterey Bay. The main conclusion from this work is that wind stress curl may result in observable cooling of the upper ocean through enhanced local upwelling when positive coherent features in stress curl are present over a significantly large area (about 20 km or more). Thus, to take into account upwelling due to stress-curl-driven Ekman pumping, the wind stress spatial variability on similar scales needs to be resolved in atmospheric and oceanic coastal models.

Inside the bay, weak atmospheric turbulence and a very shallow atmospheric boundary layer were frequently observed. We found that these characteristics are mainly due to wind sheltering by the coastal mountains, while the effects of an expansion fan play a secondary role. Consequently, near-surface winds are isolated from higher winds aloft. The weak wind forcing leads to a shallow sea surface layer and hence a warm patch of SST due to solar heating. In this area, heat balance can be a significant factor that also obscures upwelling from Ekman pumping.

REFERENCES

Banta, R. M., L. D. Olivier, and D. H. Levinson, 1993: Evolution of the Monterey Bay sea-breeze layer as observed by pulsed Doppler lidar. *J. Atmos. Sci.,* **50,** 3959–3982.

Betts, A. K., 1990: Diurnal variation of California coastal stratocumulus from two days of boundary layer soundings. *Tellus,* **42A,** 302–304.

Brooks, I. M., 2001: Air-sea interaction and the spatial variability of surface evaporation ducts in a coastal environment. *Geophys. Res. Lett.,* **28,** 2009–2012.

——, S. Söderberg, and M. Tjernström, 2003: The turbulence structure of the stable atmospheric boundary layer around a coastal headland: Aircraft observations and modeling results. *Bound.-Layer Meteor.,* **107,** 531–559.

Brost, R. A., J. C. Wyngaard, and D. H. Leschow, 1982: Marine stratocumulus layers. Part I: Mean conditions. *J. Atmos. Sci.,* **39,** 800–817.

Burk, S. D., and T. Haack, 2000: The dynamics of wave clouds upwind of coastal topography. *Mon. Wea. Rev.,* **128,** 1438–1455.

——, ——, and R. M. Samelson, 1999: Mesoscale simulation of supercritical, subcritical, and transcritical flow along coastal topography. *J. Atmos. Sci.,* **56,** 2780–2795.

Buzorius, G., J. Kalogiros, and T. Varutbangkul, 2006: Airborne aerosol flux measurements with eddy-correlation above the ocean in a coastal environment. *J. Aerosol Sci.,* **37,** 1267–1286.

Donelan, M. A., F. W. Dobson, S. D. Smith, and R. J. Anderson, 1993: On the dependence of sea surface roughness on wave development. *J. Phys. Oceanogr.,* **23,** 2143–2149.

Dorman, C. E., and C. D. Winant, 2000: The marine layer in and around the Santa Barbara Channel. *Mon. Wea. Rev.,* **128,** 261–282.

——, T. Holt, D. P. Rogers, and K. Edwards, 2000: Large-scale structure of the June–July 1996 marine boundary layer along California and Oregon. *Mon. Wea. Rev.,* **128,** 1632–1652.

Drennan, W. M., H. C. Graber, D. Hauser, and C. Quentin, 2003: On the wave age dependence of wind stress over pure wind seas. *J. Geophys. Res.,* **108,** 8062–8074.

Enriquez, A. G., and C. A. Friehe, 1995: Effects of wind stress and wind stress curl variability on coastal upwelling. *J. Phys. Oceanogr.,* **25,** 1651–1671.

——, and ——, 1997: Bulk parameterization of momentum, heat, and moisture fluxes over a coastal upwelling area. *J. Geophys. Res.,* **102** (C3), 5781–5798.

Finkelstein, P. L., and P. F. Sims, 2001: Sampling error in eddy correlation flux measurements. *J. Geophys. Res.,* **106,** 3503–3509.

Geernaert, G. L., K. B. Katsaros, and K. Richter, 1986: Variation of the drag coefficient and its dependence on sea state. *J. Geophys. Res.,* **91,** 7667–7679.

Grachev, A. A., C. W. Fairall, J. E. Hare, J. B. Edson, and S. D. Miller, 2003: Wind stress vector over ocean waves. *J. Phys. Oceanogr.,* **33,** 2408–2429.

Graham, W. M., and J. L. Largier, 1997: Upwelling shadows as near shore retention sites: The example of northern Monterey Bay. *Cont. Shelf Res.,* **17,** 509–532.

Kalogiros, J. A., and Q. Wang, 2002a: Calibration of a radome-differential GPS system on a Twin Otter research aircraft for turbulence measurements. *J. Atmos. Oceanic Technol.,* **19,** 159–171.

——, and ——, 2002b: Aerodynamic effects on wind turbulence measurements with research aircraft. *J. Atmos. Oceanic Technol.,* **19,** 1567–1576.

——, and ——, 2011: Aircraft observations of sea-surface turbulent fluxes near the California coast. *Bound.-Layer Meteor.,* **139,** 283–306, doi:10.1007/s10546-010-9585-x.

——, ——, S. R. Ramp, G. Buzorius, and H. H. Jonsson, 2006: Aircraft observations of marine boundary layer structure in the area of Monterey Bay. Preprints, *17th Symp. on Boundary Layers and Turbulence,* San Diego, CA, Amer. Meteor. Soc., 1.13. [Available online at http://ams.confex.com/ams/pdfpapers/111110.pdf.]

Kirincich, A. R., J. A. Barth, B. A. Grantham, B. A. Menge, and J. Lubchenco, 2005: Wind-driven inner-shelf circulation off central Oregon during summer. *J. Geophys. Res.,* **110,** C10S03, doi:10.1029/2004JC002611.

Kraus, E. B., and J. A. Businger, 1994: *Atmosphere-Ocean Interaction.* Oxford University Press, 362 pp.

Lentz, S. J., 2001: The influence of stratification on the wind-driven cross-shelf circulation over the North Carolina shelf. *J. Phys. Oceanogr.,* **31,** 2749–2760.

Paduan, J. D., and L. K. Rosenfeld, 1996: Remotely sensed surface currents in Monterey Bay from shore-based HF radar (Coastal Ocean Dynamics Application Radar). *J. Geophys. Res.,* **101,** 20 669–20 686.

——, and M. S. Cook, 1997: Mapping surface currents in Monterey Bay with CODAR-type HF radar. *Oceanography,* **10,** 49–52.

Pickett, M. H., and J. D. Paduan, 2003: Ekman transport and pumping in the California Current based on the U.S. Navy's high-resolution atmospheric model (COAMPS). *J. Geophys. Res.,* **108,** 3327, doi:10.1029/2003JC001902.

Ramp, S. R., J. D. Paduan, I. Shulman, J. Kindle, F. L. Bahr, and F. Chavez, 2005: Observations of upwelling and relaxation events in the northern Monterey Bay during August 2000. *J. Geophys. Res.,* **110,** C07013, doi:10.1029/2004JC002538.

——, and Coauthors, 2008: Preparing to predict: The Second Autonomous Ocean Sampling Network (AOSN-II) experiment in the Monterey Bay. *Deep-Sea Res.,* **56,** 68–86, doi:10.1016/j.dsr2.2008.08.013.

Rannik, Ü., and T. Vesala, 1999: Autoregressive filtering versus linear detrending in estimation of fluxes by the eddy covariance method. *Bound.-Layer Meteor.,* **91,** 259–280.

Rieder, K. F., J. A. Smith, and R. A. Weller, 1994: Observed directional characteristics of the wind, wind stress, and surface waves on the open ocean. *J. Geophys. Res.,* **99,** 22 589–22 596.

Rogers, D. P., and Coauthors, 1998: Highlights of Coastal Waves 1996. *Bull. Amer. Meteor. Soc.,* **79,** 1307–1326.

Rogerson, A. M., 1999: Transcritical flows in the coastal marine atmospheric boundary layer. *J. Atmos. Sci.,* **56,** 2761–2779.

Ström, L., M. Tjernström, and D. P. Rogers, 2001: Observed dynamics of coastal flow at Cape Mendocino during Coastal Waves 1996. *J. Atmos. Sci.,* **58,** 953–977.

Tjernström, M., 1999: The sensitivity of supercritical atmospheric boundary-layer flow along a coastal mountain barrier. *Tellus,* **51A,** 880–901.

——, and B. Grisogono, 2000: Simulations of supercritical flow around points and capes in a coastal atmosphere. *J. Atmos. Sci.,* **57,** 108–135.

Vickers, D., and L. Mahrt, 1997: Quality control and flux sampling problems for tower and aircraft data. *J. Atmos. Oceanic Technol.,* **14,** 512–526.

Winant, C. D., and C. E. Dorman, 1997: Seasonal patterns of surface wind stress and heat flux over the Southern California Bight. *J. Geophys. Res.,* **102,** 5641–5653.

——, ——, C. A. Friehe, and R. C. Beardsley, 1988: The marine layer off northern California: An example of supercritical channel flow. *J. Atmos. Sci.,* **45,** 3588–3605.